Aqueous Interfaces with Hydrophobic Room-Temperature Ionic Liquids: A Molecular Dynamics Study

A. Chaumont, R. Schurhammer, and G. Wipff*

Laboratoire MSM, Institut de Chimie, UMR CNRS 7551, Université Louis Pasteur, 4, rue B. Pascal, 67 000 Strasbourg, France

Received: May 30, 2005; In Final Form: July 25, 2005

We report a molecular dynamics study of the interface between water and (macroscopically) water-immiscible room-temperature ionic liquids "ILs", composed of PF_6^- anions and butyl- versus octyl-substituted methylimidazolium$^+$ cations (noted BMI^+ and OMI^+). Because the parameters used to simulate the pure ILs were found to exaggerate the water/IL mixing, they have been modified by scaling down the atomic charges, leading to better agreement with the experiment. The comparison of [OMI][PF_6] versus [BMI][PF_6] ILs demonstrates the importance of the N-alkyl substituent on the extent of solvent mixing and on the nature of the interface. With the most hydrophobic [OMI][PF_6] liquid, the "bulk" IL phase is dryer than with the [BMI][PF_6] liquid. At the interface, the OMI^+ cations retain direct contacts with the bulk IL, whereas the more hydrophilic PF_6^- anions gradually dilute in the local water micro-environment and are thus isolated from the "bulk" IL. The interfacial OMI^+ cations are ordered with their imidazolium moiety pointing toward the aqueous side and their octyl chains toward the IL side of the interface. With the [BMI][PF_6] liquid, the system gradually evolves from an IL-rich to a water-rich medium, leading to an ill-defined interfacial domain with high intersolvent mixing. As a result, the BMI^+ cations are isotropically oriented "at the interface". Because the imidazolium cations are more hydrophobic than the PF_6^- anions, the charge distribution at the interface is heterogeneous, leading to a positive electrostatic potential at the interface with the two studied ILs. Mixing−demixing simulations on [BMI][PF_6]/water mixtures are also reported, comparing Ewald versus reaction field treatments of electrostatics. Phase separation is very slow (at least 30 ns), in marked contrast with mixtures involving classical organic liquids, which separate in less than 0.5 ns at the microscopic level. The results allow us to better understand the specificity of the aqueous interfaces with hydrophobic ionic liquids, compared with classical organic solvents, which has important implications as far as the mechanism of liquid−liquid ion extraction is concerned.

Introduction

Room-temperature ionic liquids "ILs" composed of organic cations (e.g., alkyl-substituted phosphonium$^+$, pyridinium$^+$, imidazolium$^+$) and hydrophobic anions (e.g., PF_6^-, $[CF_3SO_2]_2N^-$) generally do not mix with water and can be used for liquid−liquid ion-extraction purposes. Recent applications involve the extraction of alkali and alkaline-earth cations by crown ethers or calixarenes and of actinide and lanthanide cations by phosphoryl-containing ligands. [1−5] Because of their low volatility, nonflammability, and chemical stability, ILs can be regarded as "green solvents"[6−10] that display interesting analogies with classical organic solvents used for liquid−liquid extraction purposes. Hydrophobic ILs are, however, hygroscopic and may contain a significant amount of water, which increases with the temperature, with the hydrophilic character of the anion and with a decreasing length of the alkyl substituents on the cation,[11−13] presumably also modifying the properties of their aqueous interfaces. What happens at the interface is crucial in the context of ion extraction[14] because hydrophilic ions (initially in water) and hydrophobic extractant molecules (dissolved in the IL) are expected to meet and to complex in this peculiar region. In the case of classical liquid−liquid interfaces, most of our knowledge is based on kinetic models,[15] thermodynamics,[16] electrochemical studies of ion transfer,[17] and surface spectroscopy (e.g., X-ray or neutron reflectivity[18,19] or IR studies[20−22]). Such studies are still lacking for the IL interfaces, and as quoted in a recent paper, knowledge of interfacial characteristics of ionic liquids is still poor.[23]

Computer simulations, mainly of a Monte Carlo or molecular dynamics (MD) type, have contributed to our understanding of the nature of aqueous interfaces with "classical" organic liquids,[24] of the interfacial distribution of molecular solutes[25−27] and ionic solutes,[28−32] as well as species involved in liquid−liquid ion extraction by ionophores.[33, 34] The aqueous interface with supercritical-CO_2 has been similarly explored.[34−36] Concerning ionic liquids, Gonzalez et al. investigated their surface tension,[37] whereas Lynden-Bell et al. simulated the interface between the water miscible [MMI][Cl] ionic liquid (MMI^+ = dimethylimidazolium$^+$) and Lennard−Jones fluids, water,[38] or "gas".[39] The question of water interaction with ILs has also been addressed by simulations.[40−46]

In this paper, we focus on the interface between water and [XMI][PF_6] ionic liquids, where XMI^+ stands for butylmethylimidazolium (BMI^+) or octylmethylimidazolium (OMI^+) cations (Figure 1). These ILs have been used experimentally to conduct liquid−liquid ion extraction from an aqueous phase,[10,47,48] with which they form, at the macroscopic level, a distinct phase separated by an "interface" whose nature is unknown. We

* Corresponding author. E-mail: wipff@chimie.u-strasbg.fr.

10.1021/jp052854h CCC: $30.25
Published on Web 09/17/2005

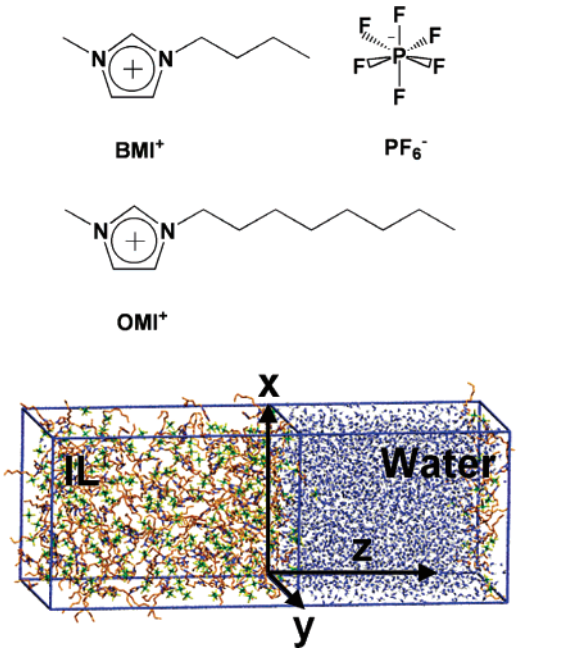

Figure 1. Simulated XMI^+ (BMI^+ and OMI^+) and PF_6^- ions and schematic representation of the IL/water interface.

analyze the interface, comparing the two ILs and, for each of them, two electrostatic models that differ by the total charge of the ionic components. For the [BMI][PF_6] IL, we compare the MD results obtained at the preformed interface with those of "demixing simulations", which started from "randomly mixed" water/[BMI][PF_6] liquids. It is indeed important to assess to what extent the liquids form distinct phases at the microscopic level and to compare the present results with those obtained with classical organic liquids.[49]

Methods

The systems were simulated by classical molecular dynamics "MD" by using the modified AMBER 7.0 software[50] in which the potential energy U is described by a sum of bond, angle, and dihedral deformation energies and pairwise additive 1−6−12 (electrostatic + van der Waals) interactions between nonbonded atoms.

$$U = \sum_{\text{bonds}} K_r(r - r_{\text{eq}})^2 + \sum_{\text{angles}} K_\theta(\theta - \theta_{\text{eq}})^2 + \sum_{\text{dihedrals}} \sum_n V_n[1 + \cos(n\phi - \gamma)] + \sum_{i<j} \left(\frac{q_i q_j}{R_{ij}} - 2\epsilon_{ij}\left(\frac{R_{ij}^*}{R_{ij}}\right)^6 + \epsilon_{ij}\left(\frac{R_{ij}^*}{R_{ij}}\right)^{12} \right)$$

Cross terms in van der Waals interactions were constructed using the Lorentz−Berthelot rules. The solvent ions were represented with all-atoms models. The BMI^+ ion parameters were taken from ref 51, whereas those of PF_6^- stem from the OPLS force field[52] and have been tested on the pure liquid properties.[51,53] The OMI^+ cation was described like BMI^+, extending the butyl chain by four neutral methylene groups, as suggested by Liu et al.[54] Two electrostatic models were considered for the ionic liquid ions: a "standard" model with total charges of +1 for XMI^+ and of −1 for PF_6^-, and a "scaled" model where all atomic charges are scaled down by 0.9. The latter procedure somewhat mimics the anion-to-cation charge transfer in the liquid.[55] When necessary, the resulting liquids will be distinguished by the notations $[XMI]^1[PF_6]^{-1}$ for the "standard" model and $[XMI]^{0.9}[PF_6]^{-0.9}$ for the "scaled" model. The standard charges and AMBER atom types are given in Figure S1. Water was described by the TIP3P model.[56] The 1−4 van der Waals interactions were scaled down by a factor of 2.0, and the 1−4 Coulombic interactions were scaled down by 1.2, as recommended by Cornell et al.[57]

The liquid systems were simulated with 3D-periodic boundary conditions. Nonbonded interactions were calculated with a 12 Å atom-based cutoff, calculating the long-range Coulombic interactions by using the Ewald summation method (PME particle−particle mesh Ewald approximation). [58] Tests with a 15 Å cutoff with a reaction field "RF" correction of electrostatics were also performed. The RF procedure assumes that the atoms within the cutoff sphere are immersed in a polarizable dielectric continuum with which they interact, leading in practice to zeroed interactions at the cutoff boundaries.[59] A dielectric constant of 80 was taken for the continuum.

The MD simulations started with random velocities and were performed at 300 K, except the "mixing" simulations (vide infra) which were run at higher temperature. The temperature was monitored by coupling the system to a thermal bath using the Berendsen algorithm[60] with a relaxation time of 0.2 ps. In the case of (NPT) simulations, the pressure was similarly coupled to a barostat[60] with a relaxation time of 0.2 ps. All C−H bonds were constrained with SHAKE,[61] using a time step of 2 fs to integrate the equations of motion.

The liquid−liquid "preformed" interface was built from two adjacent cubic boxes of IL and water, containing, respectively, ≈ 360 $BMI^+PF_6^-$ or ≈ 240 OMI^+ PF_6^- ions, and ≈ 3400 H_2O molecules (see Table 1). After 1000 steps of energy minimization, we performed 150 ps of dynamics at 300 K at a pressure of 1 atm, followed by a production step of at least 4 ns at constant volume.

Mixing−demixing MD simulations were performed on [BMI][PF_6]/water mixtures. The mixing stage started after 4 ns of dynamics at the "preformed" interface and was achieved by running 1 ns of dynamics at 600 K with biased potentials (electrostatics scaled down by a dielectric constant of 100 being used). The subsequent "demixing" simulations were performed at a temperature of 300 K, resetting the dielectric constant to one. Two different treatments of "long range" electrostatics were compared for the demixing simulations: the Ewald method as used at the preformed interface, and the reaction field "RF" method with a 15 Å cutoff.

The trajectories were saved every ps and analyzed by visual inspection of the computer graphics systems and by using our MDS software.[62] The snapshots presented here were redrawn

TABLE 1: Characteristics of the Simulated Solutions

	XMI^+	PF_6^-	water	box size (Å)	time (ns)
$[BMI]^{0.9}[PF_6]^{-0.9}$/water	363	363	3389	43.5 × 43.5 × 116.1	17.5
$[BMI]^{0.9}[PF_6]^{-0.9}$/water (demix/PME)	363	363	3389	43.5 × 43.5 × 116.1	50
$[BMI]^{0.9}[PF_6]^{-0.9}$/water (demix/RF)	363	363	3389	43.5 × 43.5 × 116.1	30
$[BMI]^1[PF_6]^{-1}$/water	363	363	3389	43.5 × 43.5 × 116.1	4.25
$[OMI]^{0.9}[PF_6]^{-0.9}$/water	240	240	3389	42.0 × 42.0 × 112	14
$[OMI]^1[PF_6]^{-1}$/water	240	240	3389	42.0 × 42.0 × 112	8

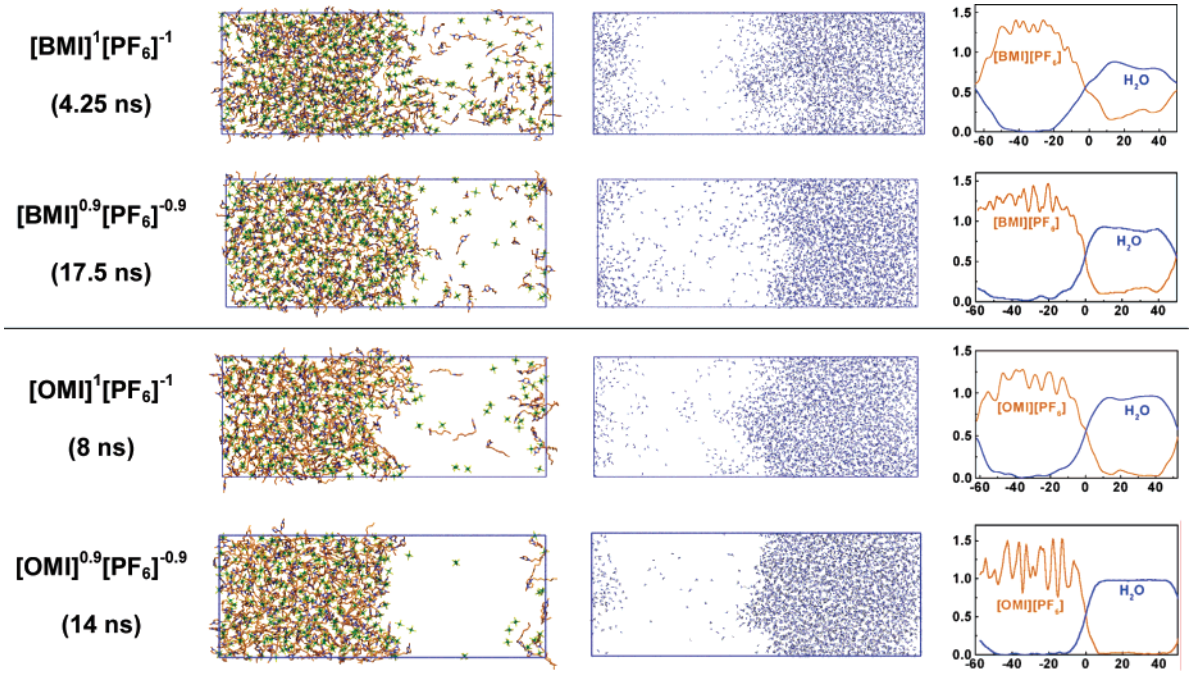

Figure 2. The aqueous interfaces of [BMI][PF_6] and [OMI][PF_6] ionic liquids. Final snapshots with water and the IL shown side by side instead of superposed for clarity. Right: density curves (averages over the last 0.5 ns of dynamics).

with the VMD software.[63] The densities of water and of the IL were calculated as a function of the *z*-coordinate in slices of $\Delta z = 0.5$ Å width (axis are defined in Figure 1), and the position of the interface ($z = 0$) was dynamically defined by the intersection of the water and IL density curves. As will be seen in the results section, some systems display significant inter-solvent mixing so that the "interfacial" and "bulk" domains are sometimes ill-defined. To be able to compare one system to the other or to describe the time evolution of a given system, we decided to define the "frontier" between the "bulk" liquid and interfacial domains at $z = \pm 12$ Å, which corresponds to about half of the interfacial width. The amount of IL in bulk water was estimated as an average of the XMI^+ and PF_6^- contributions.

The electrostatic potential $\phi(z)$ was calculated with a 17 Å + RF cutoff during the last 0.3 ns. $\phi(z)$ was obtained in *xy* slices of $\Delta z = 0.5$ Å thickness, as an average over 5×5 grids of about 81 $Å^2$ each, including the contributions of all ions and solvent atoms of the simulated box or of its nearest periodic image.

Results

We first describe the results of MD simulations which started at preformed IL/water interfaces. This is followed by the results of mixing−demixing simulations and by a discussion of the results.

1. The Aqueous Interface of [BMI][PF_6] and [OMI][PF_6] Ionic Liquids. Comparison of Two Electrostatic Models. *Solvent Mixing with the "Standard" versus "Scaled" IL Models.* During the dynamics at "preformed interfaces", the IL and water phases, initially fully separated, mixed more or less depending on the nature of the IL and of its representation. In this section, the solvent mixing in the "bulk" domains will be compared with the experimental data:[12] the molar fractions of IL in water are 1.3×10^{-3} for the [BMI][PF_6] and 3.5×10^{-4} for the [OMI]-[PF_6] ionic liquids, whereas the molar fractions of water in the IL are 0.26 for [BMI][PF_6] and 0.20 for [OMI][PF_6]. As for the calculated solubilities, they should not be overinterpreted because, in most systems, there is no clear-cut separation of

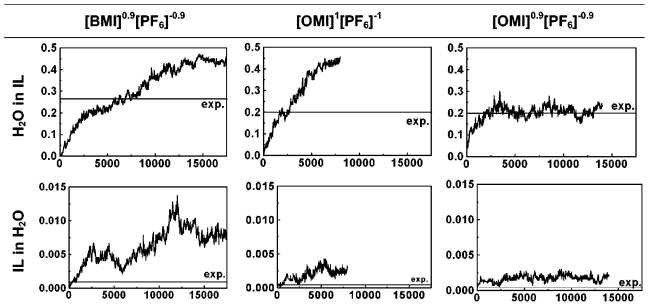

Figure 3. Simulations on the IL/water interfaces. Molar fractions of water in the IL (top) and of the IL in water (bottom) as a function of time (ps). For the [BMI][PF_6] liquid, the data cannot be represented because the interface is ill-defined due to important solvent mixing.

"bulk" and "interfacial" domains (vide infra). In addition, small numbers (as in the case of IL fraction in water [64]) generally correspond to a few ions oscillating between these "bulk" and "interfacial" domains.

Our first simulations were performed with the "standard" models $[XMI]^1[PF_6]^{-1}$ of the IL. In the case of the [BMI][PF_6] ionic liquid, such a procedure leads to significant solvent mixing and the disappearance of a well-defined interface (see Figure 2). The plot of solubilities as a function of time (Figure 3) indicates that these values are regularly increasing without reaching an equilibrium. At 4.2 ns, one finds ≈ 32 BMI^+ and PF_6^- ions in water and ≈ 100 H_2O molecules in the IL phase, which corresponds to molar fractions of, respectively, 1.8×10^{-2} and 0.30. Because the former value clearly exceeded the corresponding experimental value, this simulation was not pursued any further.

As exaggerated solvent mixing can be attributed to exaggerated IL/water interactions, we decided to rerun this simulation using the less-polar $[BMI]^{0.9}[PF_6]^{-0.9}$ model for up to 17.5 ns. This model indeed leads to reduced solvent mixing and to the formation of a more visible IL/water interface (Figure 2). After 15 ns, the system is likely to be "equilibrated", as the interliquid miscibilities seem to reach a plateau (Figure 3). The water

solubilized in the IL has a molar fraction of ≈ 0.4, which still somewhat exceeds the experimental value of 0.26,[12] whereas the IL molar fraction in the aqueous phase (≈ 0.008) is weaker than with the $[BMI]^1[PF_6]^{-1}$ model and closer to the experiment.

The $[OMI][PF_6]$/water interface was similarly simulated with the two IL models. The results (Figure 2) are consistent with the higher hydrophobicity of the OMI^+, compared to that of the BMI^+ cations, thus leading to reduced solvent mixing and to more "abrupt" interfaces when the size of imidazolium substituent increases. The time evolution of the concentrations of IL ions in water and of water in the IL (Figure 3) suggests that, with the "standard" $[OMI]^1[PF_6]^{-1}$ model, the system approaches an equilibrium at 8 ns, without reaching, however, a well-defined plateau. Because, at that time, the molar fraction of water in the IL (0.45) clearly exceeded the experimental value (0.20),[12] this simulation was not pursued any further.

When simulated with the "scaled" $[OMI]^{0.9}[PF_6]^{-0.9}$ model, the system reaches an equilibrium in less than 5 ns and does not mix further until the end of the dynamics (14 ns; see Figure 3). The corresponding molar fraction of water in the IL (0.18) is close to the experimental value. The molar fraction of IL in the aqueous phase (1.5×10^{-3}) also comes closer to the experimental value with this "scaled" rather than with the "standard" model.

Shape and Width of the Interface. The *z*-position of the interface was defined as the intersection between the solvent density curves (Figure 2). Notice that, for the bulk phases, the densities only display a well-defined plateau for water in the $[OMI]^{0.9}[PF_6]^{-0.9}$ containing system where the IL phase is quasidry, and this "plateau" gradually gets deformed when the IL becomes less hydrophobic and solubilizes in the water phase. As for the "bulk" IL, its density profile is somewhat irregular due to the large size and low mobility of the IL components.

A first look at the solvent density curves (Figure 2) indicates that the IL/water interfaces have similar widths (≈ 25−30 Å). More quantitatively, however, defining the width of the interface as the *z*-distance between the points where the solvent densities reach 90% of their "bulk" experimental values yields to the following order: $[BMI]^1[PF_6]^{-1}$ (≈ 27 Å) > $[BMI]^{0.9}[PF_6]^{-0.9}$ (20 Å) ≈ $[OMI]^1[PF_6]^{-1}$ (20 Å) > $[OMI]^{0.9}[PF_6]^{-0.9}$ (14 Å). Thus, as expected, the more hydrophobic the IL, the narrower the interface. With the most hydrophobic IL, the interface is still larger, however, than classical interfaces, e.g., ≈ 7 Å for the chloroform/water interface.[65]

The simulated interfaces are far from being instantaneously "flat" and regular. For instance, in the case of the $[OMI]^1[PF_6]^{-1}$ containing system, one can see a water cone that deeply penetrates the IL domain, and the intersolvent mixing is so great that an interface can hardly be defined (Figure 2). With the more hydrophobic $[OMI]^{0.9}[PF_6]^{-0.9}$ model, the interface is more planar on average, but instantaneously very rough. This can be seen in Figure 4, which represents the corresponding water surface, delineated by the *z*-min positions of H_2O molecules that retain contact with the bulk aqueous phase (thus excluding isolated H_2O molecules or aggregates). This surface displays dynamically exchanging troughs and mounds, whose extrema can be separated by up to ≈ 15 Å. The snapshots taken at time intervals of 100 ps illustrate the high mobility of the surface. For the other studied systems, such surfaces could not be calculated due to the interpenetration of water and ionic liquids, as illustrated in Figure 5 for the $[BMI]^{0.9}[PF_6]^{-0.9}$ interface.

Visual inspection of the trajectories shows that, during the dynamics, all interfacial OMI^+ cations retain direct contact with the bulk IL phase via, e.g., hydrophobic associations between their octyl chains or via $PF_6^-\cdots OMI^+$ ion pairing. For the interfacial PF_6^- anions, the situation is somewhat different because some form intimate ion pairs with OMI^+ cations, whereas others form solvent-separated ion pairs ($PF_6^-\cdots H_2O\cdots OMI^+$ interactions) or fully separated ion pairs. There are interfacial PF_6^- anions (at $z \approx 0$) that are surrounded by water, without direct contact with the IL phase. With the $[BMI]^{0.9}[PF_6]^{-0.9}$ liquid that involves less hydrophobic cations, there is more intersolvent mixing at the "interface". Thus, at $z \approx 0$, there are BMI^+ or PF_6^- "isolated" ions in an aqueous micro-environment, without continuous contact with the IL phase. Conversely, there are "water basins" penetrating between "isolated" BMI^+ or PF_6^- ions at the interface. Typical snapshots are presented in Figure 5. The picture is thus quite different from aqueous interfaces with classical hydrophobic liquids such as dichloroethane, chloroform, and alkanes, where the molecules of one solvent retain continuous contact with the corresponding bulk phase, leading to molecularly sharp and more "flat" interfaces (see Figure S2). In the case of ILs, the interface locally involves some fluctuating solvent mixing and is therefore more difficult to depict, especially when the IL becomes hygroscopic.

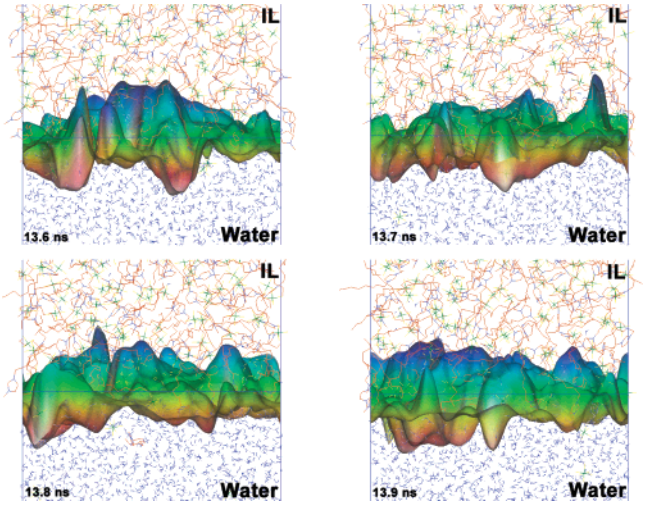

Figure 4. Water surface at the $[OMI]^{0.9}[PF_6]^{-0.9}$ interface after 13.6 ns of dynamics at time intervals of 0.1 ns. Color coded as a function of the *z*-position, between about −7 Å and +7 Å from the interface (axis are defined in Figure 1).

Orientation of Imidazolium Cations at the Interface. Another feature of interest concerns the orientation of imidazolium cations at the interface, revealing a clear difference between BMI^+ and OMI^+ containing liquids. The more hydrophobic OMI^+ cations point their alkyl chains toward the IL phase and their imidazolium ring toward water, like amphiphilic cations at classical interfaces. This can be seen in Figure 6, which represents cumulated views of the cations that sit at ±5 Å from the interface at the end of the dynamics. No such ordering is observed for the BMI^+ cations at the interface.

At the interface as well as in the bulk phases, the butyl or octyl chains of the XMI^+ cations are conformationally labile and rarely all-trans, so that the cation orientation can hardly be characterized by a single index. For simplicity, however, we decided to consider the θ angle between the *z*-axis of the box and the N−C vector connecting the N_2 atom and the terminal carbon of the alkyl chain. Figure 7 shows the populations $p(\theta)$ obtained during the last nanosecond of dynamics, selecting the cation whose N_2 atom resides for more than 0.1 ns in a slice of $\Delta z = 5$ Å width, centered at the dynamically defined interface. It can be seen that, at the $[OMI]^{0.9}[PF_6]^{-0.9}$/water interface, the distribution $p(\theta)$ of OMI^+ cations is asymmetrical and peaks at

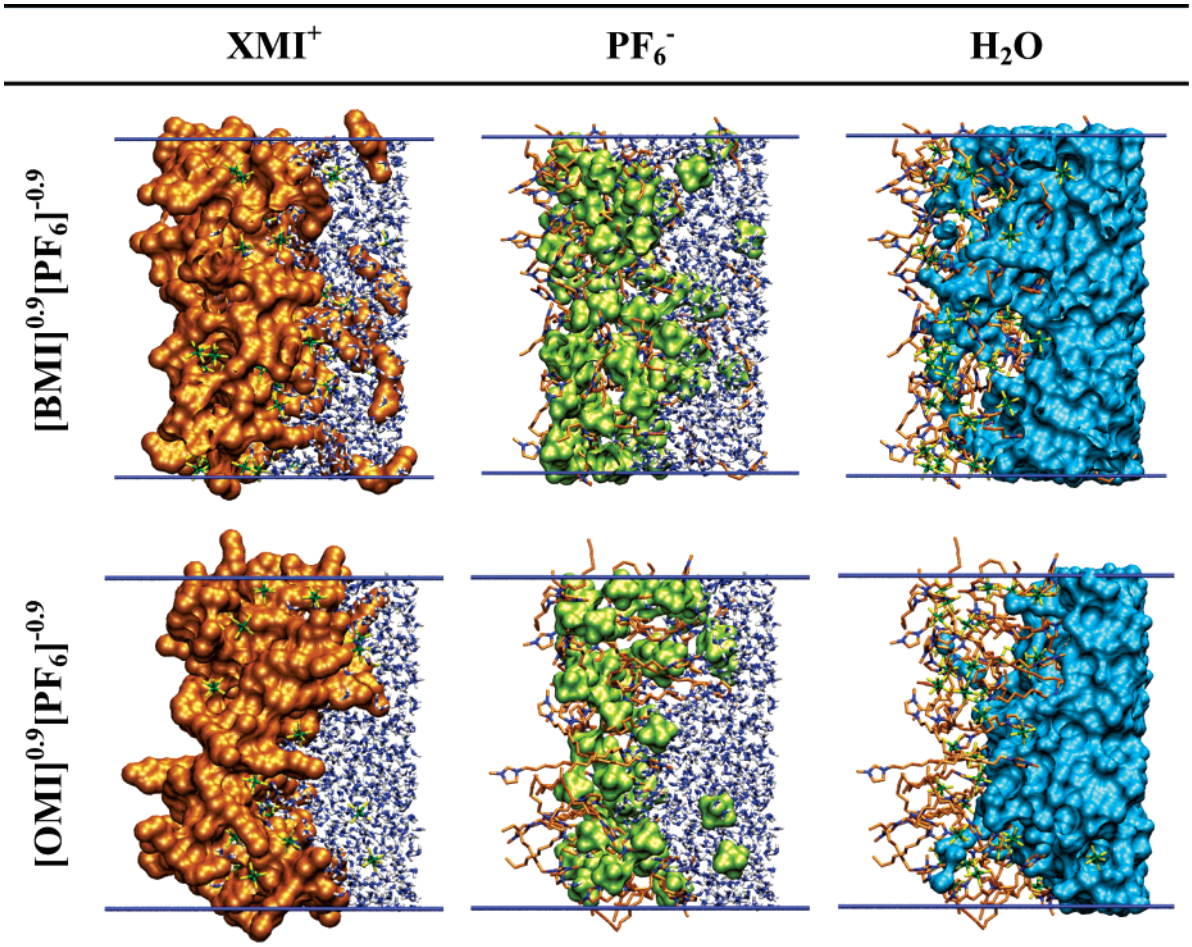

Figure 5. The $[BMI]^{0.9}[PF_6]^{-0.9}$/water and $[OMI]^{0.9}[PF_6]^{-0.9}$/water interfaces. Snapshots after 12 ns of dynamics showing the XMI^+ and PF_6^- ions and H_2O molecules, which sit within 12.5 Å from the interface.

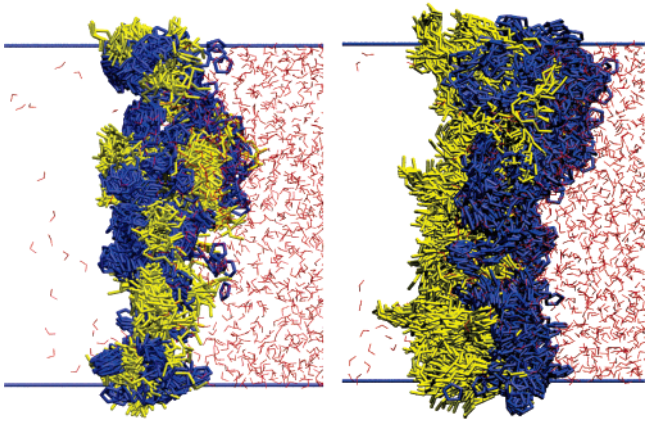

Figure 6. Imidazolium cations of the $[BMI]^{0.9}[PF_6]^{-0.9}$ (left) and $[OMI]^{0.9}[PF_6]^{-0.9}$ (right) interfaces. Cumulated views (over the last 1 ns) of the cations whose N_2 atom sits within ±5 Å from the interface at the end of the dynamics. For clarity, the other IL ions are omitted, and only one configuration of water is represented. Alkyl chains are colored in yellow, and imidazolium rings in blue.

≈ 30−40°, which confirms their marked orientation, whereas at the $[BMI]^{0.9}[PF_6]^{-0.9}$ interface, the distribution of BMI^+ cations peaks at 90° and is symmetrical, corresponding to an isotropic distribution.

Orientation may also be characterized by the order parameter S, defined by $S = 0.5\ (3\cos^2\theta - 1)$. The latter would range from 1.0, if the cations were perfectly ordered parallel to the interface, to −0.5, if they were perpendicular. A zero value of

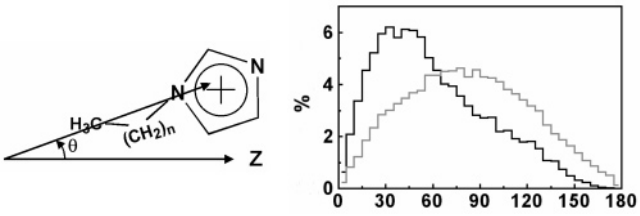

Figure 7. Orientation of imidazolium cations at the $[BMI]^{0.9}[PF_6]^{-0.9}$ (grey curve) and $[OMI]^{0.9}[PF_6]^{-0.9}$ (black curve) interfaces. Average populations $p(\theta)$ of cations which form an angle θ between the N_2-CH_3 vector of their alkyl chain and the z-axis, selecting cations that are within 5 Å from the interface during the last 3 ns.

S would correspond to an isotropic distribution. Actually, for the $[OMI]^{0.9}[PF_6]^{-0.9}$ system, the average value is $\langle S\rangle = 0.24$ (contribution of 13 OMI^+ cations) for a solvent slab centered at the interface, confirming the cation ordering. The same calculation for a slab centered on the "bulk" IL domain gives $\langle S\rangle = 0.01$ (for 20 OMI^+ cations), which indicates that the distribution is isotropic. For the $[BMI]^{0.9}[PF_6]^{-0.9}$/water system, $\langle S\rangle = 0.01$ at the interface, and −0.01 in the bulk IL, confirming that the BMI^+ cations are disordered.

Polarity of the Interface. The studied interfaces are not electrically neutral due to different distributions of XMI^+ and PF_6^- ions, and this modulates the total electrostatic potential $\phi(z)$ as a function of the z-distance from the interface (Figure 8). Splitting $\phi(z)$ into the IL and water contributions ($\phi(z) = \phi(z)^{IL} + \phi(z)^{wat}$) is instructive and reveals opposite trends. Near the interface, $\phi(z)^{IL}$ is positive and reaches a maximum because

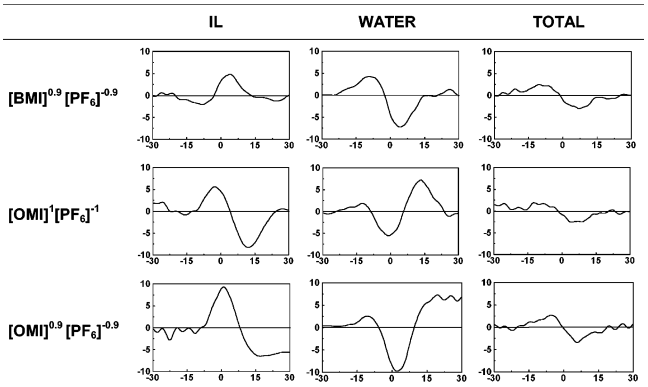

Figure 8. Neat IL/water interfaces. Average electrostatic potential $\Delta\phi(z)$ ("Total") and its components $\Delta\phi(z)^{IL}$ from the IL and $\Delta\phi(z)^{wat}$ from water as a function of the *z*-distance from the interface. Averages over the last 2 ns of dynamics.

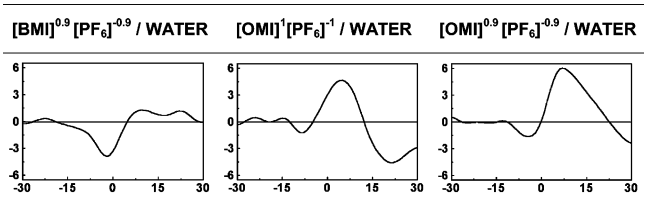

Figure 9. Neat IL/water interfaces. Total *z*-component of the H_2O dipoles as a function of the distance from the interface. Averages over the last 2 ns.

of a dominant contribution of BMI^+ or OMI^+ cations whether they are represented with standard or scaled charges. When one moves to the aqueous phase, $\phi(z)^{IL}$ decreases and becomes negative at *z* larger than 10 Å because of an excess of PF_6^- anions over XMI^+ cations on the water side. The contribution of water $\phi(z)^{wat}$ to the $\phi(z)$ potential is negative at the interface, which can be understood from the fact that the water dipoles solvate an excess of positive XMI^+ charges. On the water side, the water dipoles solvate an excess of negative charges (PF_6^- anions), leading to positive values of $\phi(z)^{wat}$. Figure 9 represents the total *z*-component of the $\mu(H_2O)$ dipoles as a function of their distance from the interface and confirms the change from negative values on the IL side to positive values on the water side of the interface, thus supporting the interpretation of the $\phi(z)^{wat}$ potentials. The sum of the $\phi(z)^{wat}$ and $\phi(z)^{IL}$ contributions leads to a net negative potential $\phi(z)$ on the water side of the interface.

Solvent Mobility in the "Bulk" Domains and at the Interface. Generally, the mobility of the H_2O, XMI^+, and PF_6^- species increases when moving from the "bulk" IL to the interface and to the aqueous phase, thus following well-known trends in increased diffusion with increased humidity of the IL.[44,66] This can be seen in Figure 10, which represents the cumulated positions of selected molecules in the IL, interfacial, and water domains of the $[OMI]^{0.9}[PF_6]^{-0.9}$/water system. This is also supported by the diffusion coefficient *D*, calculated from the Einstein equation:[67] $6\,Dt = \langle[ri(t) - ri(0)]^2\rangle$ over the last nanosecond of dynamics. The values summarized in Table 2 have been averaged over all species that reside during 1 ns in a slice of 10 Å width, centered on a given domain (bulk IL, interface or bulk water), thus excluding the species that exchange from one domain to the other. For the $[OMI]^{0.9}[PF_6]^{-0.9}$/water system, the average $\langle D\rangle$ values (in 10^{-7} cm^2 s^{-1} units) increase from 1.7 to 362 for H_2O, from 1 to 175 for PF_6^-, and from 0.9 to 56 for OMI^+ molecules. For the $[BMI]^{0.9}[PF_6]^{-0.9}$/water system, $\langle D\rangle$ increases from 2.3 to 148 for H_2O, from 1.2 to 86 for PF_6^-, and from 1.1 to 67 for BMI^+ molecules. At a given interface, the $\langle D\rangle$ coefficients are intermediate between those found in the bulk phases (Table 2). Note that the water diffusion coefficient was not calculated at the interfaces because H_2O molecules rapidly exchange between the interfacial and the bulk water domains (see Figure 10). Concerning the "bulk" IL domain of the $[BMI]^{0.9}[PF_6]^{-0.9}$ containing system, the calculated $\langle D\rangle$ coefficients are 2−3 times as high as that for the experimental values reported for the pure dry solvent (6.8 and 4.0×10^{-8} cm^2 s^{-1} for BMI^+ and PF_6^- ions, respectively, at 25 °C),[68] which is consistent with the increased diffusion when the system becomes humid.

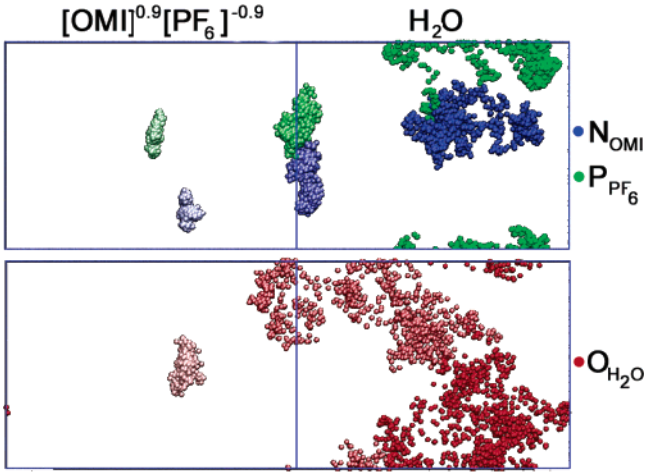

Figure 10. The $[OMI]^{0.9}[PF_6]^{-0.9}$/water interface. Cumulated views (during the last 1 ns) showing the diffusion of selected OMI^+ and PF_6^- (top) and H_2O species (bottom) from three domains (from left to right): bulk ionic liquid, interface, and bulk water. The color intensity (red for O_{H_2O}, blue for N_{OMI} and green for P_{PF_6}) increases from bulk the IL to bulk water regions.

TABLE 2: Average Diffusion Coefficients $\langle D\rangle$ (in 10^{-7} cm^2·s^{-1}) Calculated for the H_2O, PF_6^-, and XMI^+ Species in the Water, IL, and Interfacial Domains with the $[BMI]^{-0.9}[PF_6]^{0.9}$ and $[OMI]^{-0.9}[PF_6]^{0.9}$ Ionic Liquids[a]

	$[BMI]^{0.9}[PF_6]^{-0.9}$	$[OMI]^{0.9}[PF_6]^{-0.9}$
	In Water	
H_2O	148	362
XMI^+	67	56
PF_6^-	86	175
	In IL	
H_2O	2.3	1.7
XMI^+	1.1	0.9
PF_6^-	1.2	1.0
	At the Interface	
XMI^+	19.3	3.1
PF_6^-	13.1	13

[a] The averages have been obtained for 1 ns, selecting all molecules that reside during that time within a slice of 10 Å width centered on the bulk water, bulk IL, or interfacial domains.

Status of IL Ions in the Water Phase. Comparison with Pure Aqueous Solution. In the aqueous phase, the PF_6^- and imidazolium ions, although hydrophobic, rarely form intimate ion pairs and are thus most often fully hydrated. For the purpose of comparison, the BMI^+ PF_6^- and OMI^+ PF_6^- ions were simulated in water (one ion pair per water box, i.e., at a concentration of ≈ 0.04 mol/L) for 1 ns, starting with ions ≈ 13 Å apart. The resulting ion/water interaction energies E_{solv} and the cation/anion attraction energies $E_{+/-}$ plotted in Figure 11 show that the majority of configurations correspond to separated ion pairs. There are some excursions to intimate pairs,

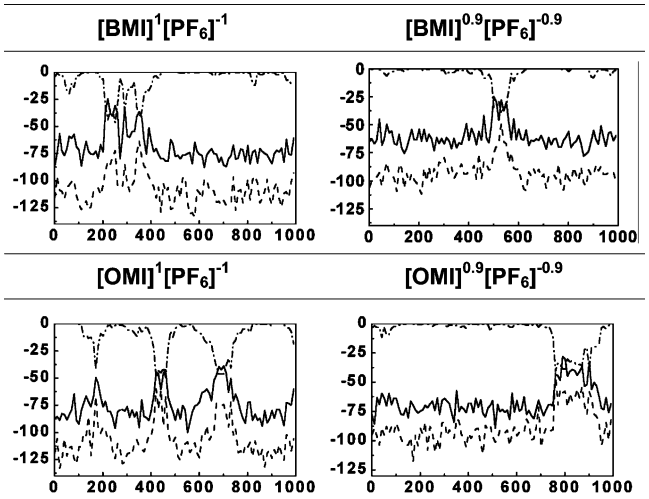

Figure 11. Simulation of the BMI^+ PF_6^- and OMI^+ PF_6^- ion pairs in water. Interaction energies (kcal/mol) as a function of time (in ps). Solid line: XMI^+/water; dashed line: PF_6^-/water; dashed−dotted line: XMI^+/PF_6^- interactions.

leading to more negative $E_{+/-}$ energies and to smaller E_{solv} energies. The PF_6^- anion is found to interact more strongly with water than the BMI^+ or OMI^+ cations do ($E_{solv} = -112$, -75, and -82 ± 6 kcal/mol, respectively, with the "standard" model and -95, -63, and -71 ± 6 kcal/mol, respectively, with the "scaled" model).[69−71] This is consistent with the higher hydrophilicity of the anions compared with the cations and may explain why the former are in excess on the aqueous side of the interface, whereas the cations are in excess at the interface.

The hydration scheme of these ions is typically hydrophobic, as seen from the radial distribution functions (RDFs) and cumulated views of first-shell water molecules (Figure S3). For the OMI^+ and BMI^+ cations, the $N_2\cdots H_{H_2O}$ and $N_2\cdots O_{H_2O}$ RDFs display a broad peak at ≈ 4.5 Å, corresponding to ≈ 20 H_2O molecules whose O−H dipoles are preferentially oriented tangential to the imidazolium moiety. The first hydration shell of PF_6^- comprises ≈ 7.5 H_2O molecules that point their protons toward the negatively charged F atoms.

2. Demixing Simulations of "Randomly Mixed" Water and [BMI][PF_6] Liquids. In this section, we examine the question of phase separation, starting from "homogeneous" mixtures of water and $[BMI]^{0.9}[PF_6]^{-0.9}$ liquids. The IL was simulated with the scaled charges that better account for the IL/water solubilities than the "standard" charges. It can be seen in Figure 12 that, at the beginning of the "demixing" simulation, the two liquids are "randomly" mixed at the microscopic level, likely more than they can be in reality.

With the ionic liquid, the phase separation turns out to be very slow and still incomplete after 10 ns of dynamics (Figure S4). At that time, one can identify some water and some IL-rich domains, but no clear phase separation. The dynamics was pushed up to 50 ns, leading to the appearance of a narrow water slab next to a broad IL slab, with still significant intersolvent mixing (Figure 12). Finally, the IL domain contains ≈ 465 H_2O molecules, which corresponds to a molar fraction of 0.7, and is thus oversaturated by a factor ≈ 2.7, compared with the experiment. Conversely, the water slab contains ≈ 18 BMI^+ and 17 PF_6^- ions IL ions, which corresponds to a molar fraction of $\approx 1.4 \times 10^{-2}$, again above the experimental value of 1.3×10^{-3}.[12] The two liquids are thus more mixed than in the simulation which started at the preformed interface, and this contrasts with what was observed with organic liquids such as chloroform,[49] dichloroethane,[72] alkanes,[73] or benzene.[74] In the case of the chloroform/water mixture, simulated in similar conditions, the two liquids separate rapidly (≈ 0.5 ns) to form two phases linked by a well-defined interface, and the latter is identical to the one obtained when the dynamics started from adjacent boxes of solvents.[49]

The above simulations were performed with Ewald summation, and one may wonder how dependent the results are on the treatment of electrostatics. This is why we decided to rerun a demixing simulation, starting from the same mixed configuration as above, but using a 15 Å cutoff + RF correction. The results show (Figures 12 and S5) that the liquids separate somewhat faster than when the Ewald summation is used. At 5 ns, one sees IL "bubbles" that are quasidry and water "bubbles" free of IL. The dynamics was pushed up to 30 ns, and at the end, distinct domains of ionic liquid and water can be recognized, but intersolvent mixing is still quite high and no "flat" interface forms between the two phases (Figure 12). The molar fractions of water in the IL (0.55) and of IL in water (4×10^{-3}) are closer to experiment than those obtained after 50 ns of dynamics with Ewald. In principle, the Ewald results are more satisfactory because they account for long-range electrostatics, but the reluctance for phase separation with Ewald may result from the imposed 3D periodicity in conjunction with too small a box size. These issues deserve further investigations. In the case of classical water/chloroform mixtures where electrostatic interactions are less important, no difference was observed between the demixing results obtained with Ewald or with the RF method.[49]

We attempted to more quantitatively describe the evolution of the phase separation by defining a demixing index λ, which would range from 1.0 for "perfectly mixed" liquids to 0.0 for fully separated liquids: $1/\lambda = 1/d_w + 1/d_{IL}$, where d_w and d_{IL} correspond to the densities of water and of the IL in the mixture. The simulation box was split in cubic boxes of 10 Å length in which the densities were calculated and averaged over the different boxes. To avoid edge effects, the procedure was repeated by shifting the origin by 5 Å. The λ values are plotted as a function of time in Figure 13. With the Ewald and RF methods, λ is initially close to 0.9 and slowly decays in a nonregular manner, to reach a plateau at ≈ 40 ns with the former method and at ≈ 30 ns with the RF method. The final values ($\lambda \approx 0.5$ and 0.4, respectively) confirm that the demixing is more advanced with the RF than with the Ewald method, as seen from the snapshots (Figure 12). However, it is not as complete as in the case of the binary chloroform/water system, for which λ decays from 1 to 0.2 in less than 0.5 ns.[49] Another difference concerns the evolution of λ, which decays regularly as a function of time with chloroform,[49] but not with the IL. In the case of ILs, the λ index sometimes increases, which is probably due to the appearance of IL-rich and water-rich ill-defined domains before the "interface" forms (Figures S4 and S5).

Discussion and Conclusions

We report an MD investigation of the aqueous interface of two ILs that form distinct phases with water at the macroscopic level. The resulting microscopic views reveal marked differences, compared with classical organic interfaces, due to the ionic nature of the "hydrophobic" phase and to differences in the XMI^+ versus PF_6^- ion partitioning. The comparison of two imidazolium-based ILs further demonstrates the effect of the IL cation on the interfacial landscape. These simulations are

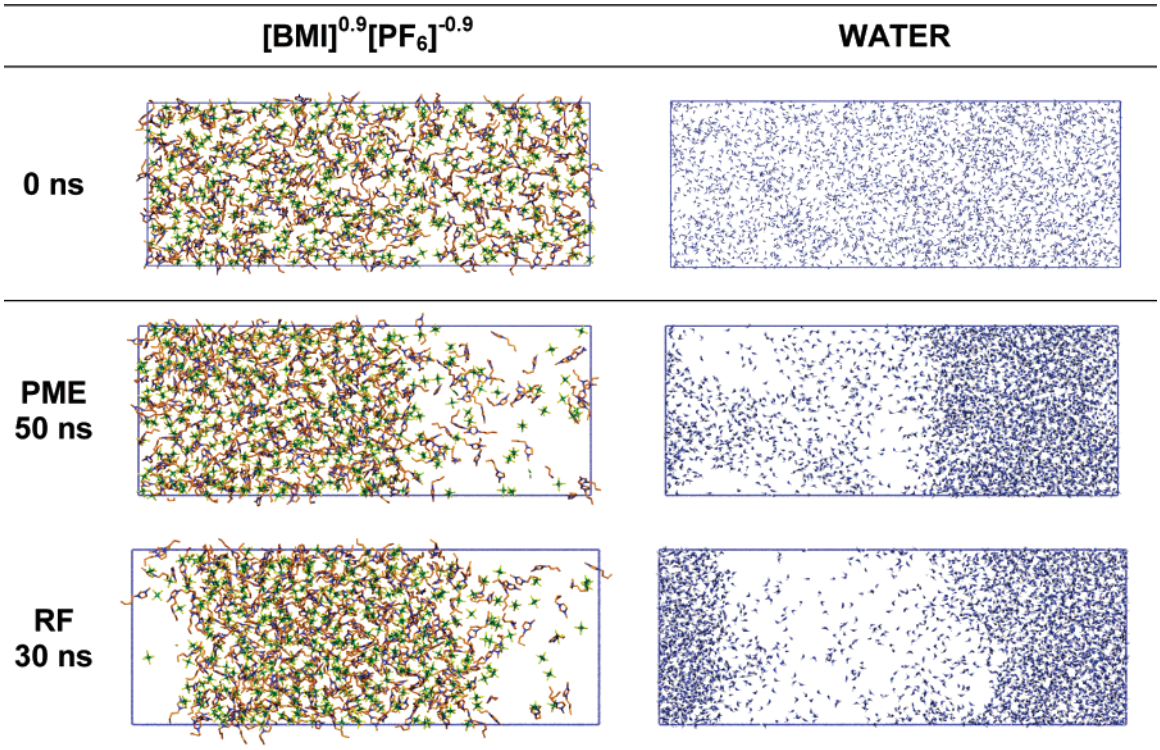

Figure 12. Phase separation of "randomly mixed" $[BMI]^{0.9}[PF_6]^{-0.9}$/water liquids, calculated with Ewald (PME) vs reaction field (RF) treatment of electrostatics. Initial and final views, with liquids shown side by side instead of superposed for clarity. A full version is given in Figures S4 and S5.

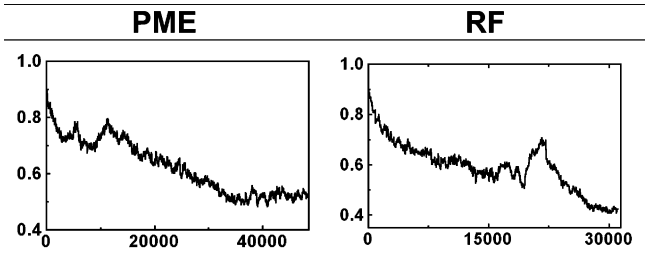

Figure 13. Phase separation of the "randomly mixed" $[BMI]^{0.9}[PF_6]^{-0.9}$/water system. Demixing index λ as a function of time (ps) from MD simulations performed with PME and RF treatments of electrostatics.

exploratory in nature and cannot claim to be quantitative. One important issue concerns the force field representation of the different partners, and this will be addressed in the following, in conjunction with other methodological issues. This will be followed by a discussion of the characteristics of the interface with implications in the context of assisted ion transfer from water to the IL.

On the Representation of Ionic Liquids and Water at the Interface. Following procedures that are common for classical liquid−liquid interfaces, we used solvent parameters developed for the neat liquids to study their interfaces. Concerning the ILs, the parameters were derived from existing force fields, complemented by *ab* initio QM calculations.[51,54,55,75−80] We can note that the interaction energy between the BMI^+ and PF_6^- ions calculated with AMBER (−75.9 kcal/mol) nicely agrees with QM results (−76.2 and −76.8 kcal/mol, respectively[53,54]). Interaction energies with water are also well described by AMBER, compared with HF/6-31+G* or DFT-B3LYP/6-31+G* results. These are −10.4, −9.1, and −9.1 kcal/mol, respectively, for the $PF_6^-\cdots H_2O$ dimer and −9.2, −9.7, and −9.5 kcal/mol, respectively, for the $BMI^+\cdots OH_2$ dimer ($C_2H\cdots OH_2$ hydrogen bond).[43,81] Meeting such criteria is not sufficient, however, to correctly depict aggregates,[82] condensed phases, or solvent mixtures because of many-body, charge-transfer, and polarization effects.[43,81] Our results based on "standard" IL parameters indeed indicate that the IL/water affinities are exaggerated, and this should also be the case with other recently reported models.

TABLE 3: Average Interaction Energies (in kcal/mol) of BMI^+ and PF_6^- Ions and Pure TIP3P Water, Obtained with Four Electrostatic Representations of the Ions

	A-scaled[a]	**A**-standard[a]	**B**[b]	**C**[c]
BMI^+/water	−63 ± 7	−75 ± 6	−77 ± 7	−74 ± 8
PF_6^-/water	−95 ± 6	−112 ± 10	−116 ± 6	−115 ± 9

[a] Parameters used in this work. [b] Charges from ref 83. [c] Charges from ref 54.

We indeed compared the average interaction energies E_{solv} of BMI^+ and PF_6^- ions and water, calculated with our charge models (noted **A** (standard) and **A** (scaled)) and with two other charge distributions based on 1−6−12 potentials: the models **B** from Lopes et al.[83] and **C** from Liu et al.[54] For this purpose, we simulated the BMI^+ PF_6^- ion pair in bulk water (TIP3P model) for 1 ns, starting with dissociated ions. The results (Table 3) show that the **B** and **C** models give, within statistical fluctuations, similar E_{solv} energies as our **A**(standard) model and would also exaggerate the IL/water mixing. This is why we scaled down the charges, thereby reducing the E_{solv} energy by ≈15% (Table 3) and thus reducing the intersolvent mixing in the binary IL/water systems.

The interfacial properties may also depend on the water model. The TIP3P water model used throughout this study for computational efficiency is known to somewhat overestimate the polarity of water at hydrophobic surfaces or at the water/air interfaces,[84] but this issue is expected to be less important at interfaces with ionic liquids, which are more polar. What happens with other water models, especially those including

polarization,[85] remains to be investigated and requires further consistent parameter developments for the ionic liquid and, in practice, important computational resources, to attain the simulated time scales.

The sampling issue is very important and cannot be overlooked, as seen particularly in the case of the $[BMI]^{0.9}[PF_6]^{-0.9}$/water system. Despite the long simulated times, the simulations that started either from a preformed interface or from "randomly mixed" liquids did not converge toward identical distributions, and this contrasts with what has been found with a classical organic solvent.[49] The "bulk" IL phase is more humid after 50 ns of demixing simulations than it is after 17 ns of dynamics at the preformed interface. Because of computer time limitations, the latter simulation was not pursued any further. Both simulations show that the IL is quite viscous and, although forming a macroscopically separated phase with water, hygroscopic. On the other hand, the fact that the IL and water liquids separate in about 50 ns suggests that they are unlikely to form homogeneous mixtures at the microscopic level when they are shaken together, as in a typical liquid−liquid extraction experiment.

Despite the lack of full convergence of the simulations that started from different configurations, we believe that the results obtained in the same conditions allow for consistent comparisons. They clearly indicate that the IL/water interfaces are broader and involve more solvent mixing than classical interfaces and that their width increases when the IL becomes more hygroscopic, i.e., from $[OMI][PF_6]$ to $[BMI][PF_6]$.

On the Orientation of Imidazolium Ions at the Aqueous Interface. Our comparison of BMI^+ and OMI^+ based ILs shows differences in the cation orientations at the interface. To our knowledge, there are no experimental data on the structure of the studied interfaces, whereas a few studies focused on the orientation of imidazolium cations at the IL/air interfaces.[86−88] The latter differ a priori from IL/water interfaces because the ILs are nonvolatile and do not interact with air, whereas they can strongly interact with water. Surface tension and direct recoil spectrometric data indicated that the surface of the IL is shared by the imidazolium cations and the anions (PF_6^- or BF_4^-) and that the orientation of the cations depends on the length of their alkyl substituents.[87] Another study, on the basis of sum frequency generation vibrational spectroscopy, compared the surfaces of ILs, first dry, and then under some water pressure, and the results are therefore more relevant for the IL/water interface.[88] Interestingly enough, it was found that the surface of hydrophobic, nonmiscible ionic liquids is more sensitive to the addition of water than the surface of hydrophilic ionic liquids. When contacted with water, hydrophobic ILs respond by reorienting their cations to help solvate the water molecules.[88] This is consistent with the marked orientation of cations found in our simulations at the $[OMI][PF_6]$ interface, which contrasts with the isotropic distribution of cations at the $[BMI][PF_6]$ interface.

Polarity of the Ionic Liquid/Water and Implications for the Ion-Extraction Mechanisms. According to the simulations, the interface is not neutral, but positively charged, because of a small excess of imidazolium cations, compensated by a small excess of PF_6^- anions in the aqueous phase. This may be important in the context of M^{n+} ions extraction from water because the negative potential on the aqueous side attracts M^{n+} cations, thereby increasing their concentration and facilitating their complexation and transfer to the IL phase.

The solubility of XMI^+ cations in water is another important factor. In classical M^{n+} cation extraction, the neutrality of the system is generally achieved via co-extraction of nX^- anions from water or via the exchange of n protons of ionizable extractant molecules. In the case of ILs, neutrality may be achieved by another mechanism, exchanging M^{n+} with n solvent (e.g., imidazolium) cations,[3,89] which implies that the latter diffuse from the interface to water. Comparison of $[OMI]^{0.9}[PF_6]^{-0.9}$ with $[BMI]^{0.9}[PF_6]^{-0.9}$ interfaces shows that the concentration of IL ions dissolved in water increases from ≈ 0.001 to 0.008 mol/L. This is consistent with the evolution from an anion co-extraction mechanism with the $[OMI][PF_6]$ liquid to a cation-exchange mechanism with $[BMI][PF_6]$, as suggested by experiment.[13,89−92] Also, note that the interface is broader and involves more local solvent mixing with the latter liquid, which should lower the interfacial pressure and facilitate the interface crossing. These simulation results should stimulate further theoretical and experimental studies on the studied and related interfacial systems.

Acknowledgment. We are grateful to IDRIS, CINES, Université Louis Pasteur, and PARIS for computer resources and to E. Engler for assistance.

Supporting Information Available: $[BMI][PF_6]$ and $[OMI][PF_6]$ interfaces; Atomic charges and AMBER atom types of the simulated BMI^+, OMI^+ and PF_6^- ions; The chloroform/water interface; $BMI^{+0.9}$, $OMI^{+0.9}$, and $PF_6^{-0.9}$ ions in water; Phase separation of "randomly mixed" $[BMI]^{0.9}[PF_6]^{-0.9}$/water liquids. This material is available free of charge via the Internet at http://pubs.acs.org.

References and Notes

(1) Visser, A. E.; Rogers, R. D. *J. Solid State Chem.* **2003**, *171*, 109−113.
(2) Dai, S.; Shin, Y. S.; Toth, L. M.; Barnes, C. E. *Inorg. Chem.* **1997**, *36*, 4900−4902.
(3) Visser, A. E.; Swatloski, R. P.; Griffin, S. T.; Hartman, D. H.; Rogers, R. D. *Sep. Sci. Technol.* **2001**, *36*, 785−804.
(4) Visser, A. E.; Swatlosli, R. P.; Reichert, W. M.; Mayton, R.; Sheff, S.; Wierzbicki, A.; Davies, J.; Rogers, R. D. *Environ. Sci. Technol.* **2002**, *36*, 2523−2529.
(5) Luo, H.; Dai, S.; Bonnesen, P. V.; Buchanan, A. C., III; Holbrey, J. D.; Bridges, N. J.; Rogers, R. D. *Anal. Chem.* **2004**, *76*, 3078−3083.
(6) Swatloski, R. P.; Holbrey, J. D.; Rogers, R. D. *Green Chem.* **2003**, *5*, 361−363.
(7) Welton, T. *Chem. Rev.* **1999**, *99*, 2071−2083.
(8) Wasserscheid, P.; Welton, T. *Ionic Liquids in Synthesis*; Wiley-VCH: Weinheim, 2002.
(9) Huddleston, J. G.; Willauer, H. D.; Swatloski, R. P.; Visser, A. E.; Rogers, R. D. *Chem. Comm.* **1998**, 1765−1766.
(10) Rogers, R. D.; Seddon, K. R. *Science* **2003**, *302*, 792.
(11) Seddon, K. R.; Stark, A.; Torres, M. J. *Pure Appl. Chem.* **2000**, *72*, 2275−2287.
(12) Anthony, J. L.; Maginn, E. J.; Brennecke, J. F. *J. Phys. Chem. B* **2001**, *105*, 10942−10949.
(13) Huddleston, J. G.; Visser, A. E.; Reichert, W. M.; Willauer, H. D.; Broker, G. A.; Rogers, R. D. *Green Chem.* **2001**, *3*, 156−164.
(14) Watarai, H. *Trend Anal. Chem.* **1993**, *12*, 313−318.
(15) Danesi, P. R. In *Principles and Practices of Solvent Extraction*; Rydberg, J., Musikas, C., Choppin, G. R., Ed.; Dekker: New York, 1992; pp 157−207.
(16) Schmickler, W. *Interfacial Electrochemistry*; Oxford University Press: New York, 1996.
(17) Girault, H. H.; Schiffrin, D. J. In *Electroanalytical Chemistry*; Bard, A. J. Ed.; Dekker: New York, 1989; pp 1−141 and references therein.
(18) Mitrinovic, D. M.; Zhang, Z.; Williams, S.; Huang, Z.; Schlossman, M. L. *J. Phys. Chem. B* **1999**, *103*, 1779−1782.
(19) Mitrinovic, D. M.; Tikhonov, A. M.; Li, M.; Huang, Z.; Schlossman, M. L. *Phys. Rev. Lett.* **2000**, *85*, 582−585.
(20) Eisenthal, K. B. *Chem. Rev.* **1996**, *96*, 1343−1360.
(21) Conboy, J. C.; Richmond, G. L. *J. Phys. Chem. B* **1997**, *101*, 983−990.
(22) Fitchett, B. D.; Knepp, T. N.; Conboy, J. C. *J. Electrochem. Soc.* **2004**, *151*, E219−E225.

(23) Halka, V.; Tsekov, T.; Freyland, W. *Phys. Chem. Chem. Phys.* **2005**, *7*, 2038−2043.
(24) Benjamin, I. *Annu. Rev. Phys. Chem.* **1997**, *48*, 407−451 and references therein.
(25) Chipot, C.; Wilson, M. A.; Pohorille, A. *J. Phys. Chem. B* **1997**, *101*, 782−791.
(26) Sokhan, V. P.; Tildesley, D. J. *Faraday Discuss.* **1996**, *104*, 193−208.
(27) Pohorille, A.; Benjamin, I. *J. Phys. Chem.* **1993**, *97*, 2664−2670.
(28) Wilson, M. A.; Pohorille, A. *J. Chem. Phys.* **1991**, *95*, 6005−6013.
(29) Benjamin, I. *Chem. Rev.* **1996**, *96*, 1449−1475.
(30) Dang, L. X. *J. Phys. Chem. B* **1999**, *103*, 8195−81200.
(31) Spohr, E.; Heinzinger, K. *Electrochim. Acta* **1988**, *33*, 1211−1222.
(32) Schweighofer, K. J.; Essmann, U.; Berkowitz, M. *J. Phys. Chem. B* **1997**, *101*, 3793−3799.
(33) Wipff, G.; Lauterbach, M. *Supramol. Chem.* **1995**, *6*, 187−207.
(34) Baaden, M.; Schurhammer, R.; Wipff, G. *J. Phys. Chem. B* **2002**, *106*, 434−441.
(35) Schurhammer, R.; Berny, F.; Wipff, G. *Phys. Chem. Chem. Phys.* **2001**, *3*, 647−656.
(36) da Rocha, S. R. P.; Johnston, K. P.; Westacott, R. E.; Rossky, P. J. *J. Phys. Chem. B* **2001**, *105*, 12092−12104.
(37) Gonzalez-Melchor, M.; Bresme, F.; Alejandre, J. *J. Chem. Phys.* **2005**, *122*, 104710.
(38) Lynden-Bell, R. M.; Kohanoff, J.; Popolo, M. G. D. *Faraday Discuss.* **2005**, *129*/*5*, 1−11.
(39) Lynden-Bell, R. M. *Mol. Phys.* **2003**, *101*, 2625−2633.
(40) Hanke, C. G.; Atamas, N. A.; Lynden-Bell, R. M. *Green Chem.* **2002**, *4*, 107−111.
(41) Lynden-Bell, R. M.; Atamas, N. A.; Vasilyuk, A.; Hanke, C. G. *Mol. Phys.* **2002**, *100*, 3225−3229.
(42) Hanke, C. G.; Lynden-Bell, R. M. *J. Phys. Chem. B* **2003**, *107*, 10873−10878.
(43) Chaumont, A.; Wipff, G. *Inorg. Chem.* **2004**, *43*, 5891−5901.
(44) Vayssière, P.; Chaumont, A.; Wipff, G. *Phys. Chem. Chem. Phys.* **2004**, *7*, 124−135.
(45) Deschamps, J.; Gomes, M. F. C.; Padua, A. A. H. *ChemPhysChem* **2004**, *5*, 1049−1052.
(46) Shah, J. K.; Maginn, E. J. *J. Phys. Chem. B* **2005**, *109*, 10395−10405.
(47) Wei, G. T.; Yang, Z.; Chen, C. J. *Anal. Chim. Acta* **2003**, *488*, 183−192.
(48) Nakashima, K.; Kubota, F.; Maruyama, T.; Goto, M. *Anal. Sci.* **2003**, *19*, 1097−1098.
(49) Muzet, N.; Engler, E.; Wipff, G., *J. Phys. Chem. B* **1998**, *102*, 10772−10788.
(50) Case, D. A.; Pearlman, D. A.; Caldwell, J. W.; Cheatham, T. E., III; Wang, J.; Ross, W. S.; Simmerling, C. L.; Darden, T. A.; Merz, K. M.; Stanton, R. V.; Cheng, A. L.; Vincent, J. J.; Crowley, M.; Tsui, V.; Gohlke, H.; Radmer, R. J.; Duan, Y.; Pitera, J.; Massova, I.; Seibel, G. L.; Singh, U. C.; Weiner, P. K.; Kollman, P. A. *AMBER7*; University of California: San Francisco, 2002.
(51) de Andrade, J.; Böes, E. S.; Stassen, H., *J. Phys. Chem. B* **2002**, *106*, 13344−13351.
(52) Kaminski, G. A.; Jorgensen, W. L. *J. Chem. Soc., Perkin Trans. 2* **1999**, *2*, 2365−2375.
(53) Chaumont, A.; Engler, E.; Wipff, G. *Inorg. Chem.* **2003**, *42*, 5348−5356.
(54) Liu, Z.; Huang, S.; Wang, W. *J. Phys. Chem. B* **2004**, *108*, 12978−12989.
(55) Morrow, T. I.; Maginn, E. J. *J. Phys. Chem. B* **2002**, *106*, 12807−12813.
(56) Jorgensen, W. L.; Chandrasekhar, J.; Madura, J. D.; Impey, R. W.; Klein, M. L. *J. Chem. Phys.* **1983**, *79*, 926−936.
(57) Cornell, W. D.; Cieplak, P.; Bayly, C. I.; Gould, I. R.; Merz, K. M.; Ferguson, D. M.; Spellmeyer, D. C.; Fox, T.; Caldwell, J. W.; Kollman, P. A. *J. Am. Chem. Soc.* **1995**, *117*, 5179−5197.
(58) Darden, T. A.; York, D. M.; Pedersen, L. G. *J. Chem. Phys.* **1993**, *98*, 10089.
(59) Tironi, I. G.; Sperb, R.; Smith, P. E.; van Gunsteren, W. F. *J. Chem. Phys.* **1995**, *102*, 5451−5459.
(60) Berendsen, H. J. C.; Postma, J. P. M.; van Gunsteren, W. F.; DiNola, A. *J. Chem. Phys.* **1984**, *81*, 3684−3690.
(61) Ryckaert, J. P.; Ciccotti, G.; Berendsen, H. J. C. *J. Comput. Phys.* **1977**, *23*, 327−336.
(62) Engler, E.; Wipff, G. In *Crystallography of Supramolecular Compounds*; Tsoucaris, G. Ed.; Kluwer: Dordrecht, 1996; pp 471−476.
(63) Humphrey, W.; Dalke, A.; Schulten, K. *J. Mol. Graphics* **1996**, *14*, 33−38.
(64) If there were no solvent mixing, a single XMI^+ PF_6^- ion pair in the simulated water box would correspond to a molar fraction of 4×10^{-4}.
(65) Wipff, G.; Engler, E.; Guilbaud, P.; Lauterbach, M.; Troxler, L.; Varnek, A. *New J. Chem.* **1996**, *20*, 403−417.
(66) Schröder, U.; Wadhawan, J. D.; Compton, R. G.; Marken, F.; Suarez, P. A. Z.; Consorti, C. S.; Souza, R. F. D.; Dupont, J. *New. J. Chem.* **2000**, *24*, 1009−1015.
(67) Allen, M. P.; Tildesley, D. J. *Computer Simulation of Liquids*; van Gunsteren, W. F., Weiner, P. K., Ed.; Clarendon Press: Oxford, 1987, p 60.
(68) Tokuda, H.; Hayamizu, K.; Ishii, K.; Susan, M. A. B. H.; Watanabe, M. *J. Phys. Chem. B* **2004**, *108*, 16593−16600.
(69) Concerning the BMI^+ vs PF_6^- comparison, the anion is more hydrophilic because it interacts better with water and because of its smaller size, leading to a smaller cavitation energy in water (14 and 26 kcal/mol, respectively, for PF_6^- and BMI^+). Concerning the OMI^+ vs BMI^+ comparison, the change in cavitation energies (35 vs 26 kcal/mol, respectively) compensates for the better interactions of the former cation with water. Estimations from HF calculations with 6-31+G* basis and the PCM model implemented in Gaussian-98.[71]
(70) Comparing the two electrostatic models of the ions shows that scaling down the charges by 0.9 has a similar influence on the PF_6^- anions as on the BMI^+ or OMI^+ cations: their interaction energy with water decreases by 14, 15, and 13%, respectively.
(71) Frisch, M. J.; Trucks, G. W.; Schlegel, H. B.; Scuseria, G. E.; Robb, M. A.; Cheeseman, J. R.; Zakrzewski, V. G.; Montgomery, J. A., Jr.; Stratmann, R. E.; Burant, J. C.; Dapprich, S.; Millam, J. M.; Daniels, A. D.; Kudin, K. N.; Strain, M. C.; Farkas, O.; Tomasi, J.; Barone, V.; Cossi, M.; Cammi, R.; Mennucci, B.; Pomelli, C.; Adamo, C.; Clifford, S.; Ochterski, J.; Petersson, G. A.; Ayala, P. Y.; Cui, Q.; Morokuma, K.; Malick, D. K.; Rabuck, A. D.; Raghavachari, K.; Foresman, J. B.; Cioslowski, J.; Ortiz, J. V.; Stefanov, B. B.; Liu, G.; Liashenko, A.; Piskorz, P.; Komaromi, I.; Gomperts, R.; Martin, R. L.; Fox, D. J.; Keith, T.; Al-Laham, M. A.; Peng, C. Y.; Nanayakkara, A.; Gonzalez, C.; Challacombe, M.; Gill, P. M. W.; Johnson, B. G.; Chen, W.; Wong, M. W.; Andres, J. L.; Head-Gordon, M.; Replogle, E. S.; Pople, J. A. *Gaussian 98*, revision A.5; Gaussian, Inc.: Pittsburgh, PA, 1998.
(72) Schweighofer, K. J.; Benjamin, I. *J. Phys. Chem.* **1995**, *99*, 9974−9985.
(73) Carpenter, I. L.; Hehre, W. J. *J. Phys. Chem.* **1990**, *94*, 531−536.
(74) Linse, P. *J. Chem. Phys.* **1987**, *86*, 4177−4187.
(75) Hanke, C. G.; Price, S. L.; Lynden-Bell, R. M. *Mol. Phys.* **2001**, *99*, 801−809.
(76) Morrow, T. I.; Maginn, E. J. *J. Phys. Chem. B* **2003**, *107*, 9160.
(77) Shah, J. K.; Brennecke, J. F.; Maginn, E. J. *Green Chem.* **2002**, *4*, 112−118.
(78) de Andrade, J.; Böes, E. S.; Stassen, H. *J. Phys. Chem. B* **2002**, *106*, 3546−3548.
(79) Canongia-Lopes, J. N.; Deschamps, J.; Padua, A. A. H. *J. Phys. Chem. B* **2004**, *108*, 2038−2047.
(80) Shah, J. K.; Maginn, E. J. *Fluid Phase Equilib.* **2004**, *4*, 195−203.
(81) Although one H_2O molecule displays similar interactions with one PF_6^- or one BMI^+ ion in the gas phase, in the humid $[BMI][PF_6][H_2O]$ liquid, one H_2O molecule was found to interact more with PF_6^- anions than with the BMI^+ cations (−7.7 and −3.0 kcal/mol, respectively, on the average).[43] This suggests that the favored hydration of PF_6^- in the ionic liquid results from entropy effects due to the larger accessible surface of PF_6^-, compared with the restricted binding C_2H region of BMI^+ ions. We also note that the experimental enthalpy of water absorption by the [BMI][PF_6] liquid (7.2 kcal/mol; see ref 12) is smaller than the individual $PF_6^-\cdots H_2O$ or $BMI^+\cdots OH_2$ interaction energies calculated in the gas phase.
(82) Caldwell, J.; Dang, L. X.; Kollman, P. A. *J. Am. Chem. Soc.* **1990**, *112*, 9144−9147.
(83) Lopes, J. N. C.; Deschamps, J.; Padua, A. A. H. *J. Phys. Chem. B* **2004**, *108*, 2038−2047.
(84) Chang, T. M.; Dang, L. X. *J. Chem. Phys.* **1995**, *104*, 6772−6783.
(85) Dang, L. X. *J. Phys. Chem. B* **2001**, *105*, 804−809.
(86) Rivera-Rubero, S.; Baldelli, S. *J. Am. Chem. Soc.* **2004**, *126*, 11788−11789.
(87) Law, G.; Watson, P. R. *Chem. Phys. Lett.* **2001**, *345*, 1−4.
(88) Baldelli, S. *J. Phys. Chem. B* **2003**, *107*, 6148−6152.
(89) Visser, A. E.; Swatloski, R. P.; Reichert, W. M.; Griffin, S. T.; Rogers, R. D. *Ind. Eng. Chem. Res.* **2000**, *39*, 3596−3604.
(90) Visser, A. E.; Swatloski, R. P.; Rogers, R. D. *Green Chem.* **2000**, *2*, 1.
(91) Jensen, M. P.; Neuenfeind, J.; Beitz, J. V.; Skanthakumar, S.; Sonderholm, L. *J. Am. Chem. Soc.* **2003**, *125*, 15466−15473.
(92) Dietz, M. L.; Dzielawa, J. A.; Laszak, I.; Young, B. A.; Jensen, M. P. *Green Chem.* **2003**, *5*, 682−685.